Calculating Characteristics of Non-collinear Phase-matching in Uniaxial and Biaxial Crystals

N. Boeuf, D. Branning, I. Chaperot, E. Dauler, S. Guérin, G. Jaeger, A. Muller, A. Migdall

Optical Technology Division, 100 Bureau Dr. Stop 8441
National Institute of Standards and Technology
Gaithersburg, MD 20899-8441, U.S.A

Tel. (301) 975-2331, FAX (301) 975-2950

Amigdall@nist.gov

Web page:

http://physics.nist.gov/Divisions/Div844/facilities/cprad/cprad.html

Abstract

A method of calculating the characteristics of non-collinear phase-matching in both uniaxial and biaxial crystals is presented. Although significant work has been done to characterize collinear phase-matching and to present many of its applications, non-collinear phase-matching also has unique characteristics, leading to several useful applications. The method presented here allows calculations of both the collinear and non-collinear cases, and allows a far larger set of nonlinear crystals and configurations to be studied.

I. Introduction

The process of spontaneous parametric downconversion, in which a "pump" photon is effectively split into a pair of lower-energy "signal" and "idler" photons in a nonlinear optical medium, has proved abundantly useful in the last decade. The twin photons, which are entangled in energy, momentum, and emission time, have been used in a variety of striking demonstrations of the most nonclassical aspects of quantum theory [1,2]. In addition, the downconverted photons have found applications in the field of metrology, where they can be used to determine the quantum efficiency of photon-counting detectors, and also to determine the spectral radiance of an infrared source. The photon correlations of down-converted light allow these measurement applications to be performed in a fundamentally absolute manner as opposed to conventional methods which rely on previously calibrated standards [3,4].

Calculation of the three-wave downconversion interaction requires the use of conservation of energy and conservation of momentum, commonly referred to as phase-matching. Because the process is nonresonant, a downconverted photon may be emitted over a wide range of wavelengths, so long as the energy and momentum conservation conditions for the pair of photons are met. The individual photons of a pair may also propagate along different directions, this is referred to as *non-collinear* phase-matching. Collinear phase-matching, where the incident photon and the output pair of photons propagate in the same direction inside the crystal, is generally well understood, while the non-collinear geometry is more difficult to calculate and thus is poorly documented. One of the advantages of non-collinear phase-matching over the collinear case is that it allows easy discrimination between each of the two downconverted photons and the pump beam.

In this paper, we will describe a broadly applicable method of finding non-collinear phase-matching configurations. We also provide examples obtained from a computer program we have developed that implements our method and is freely available on the Internet. We hope that the broad pool of calculable crystal data included with this program (both uniaxial and biaxial crystals are included) and wide spectral ranges that can now be calculationally investigated will aid other researchers in designing their parametric downconversion experiments.

II. Theory: phase-matching conditions in uniaxial and biaxial crystals

II. 1. Coordinate system, equations and variables

Consider a three-wave mixing process, where one photon incident on the crystal interacts to produce a pair of lower-energy correlated photons by parametric downconversion. This study is carried out for the most general case, including biaxial and uniaxial crystals, for non-collinear or collinear geometries and for pairs of downconverted photons with or without equal frequencies. The two main constraints are the conservation of energy,

$$\omega_{\text{Pump}} = \omega_{\text{Signal}} + \omega_{\text{Idler}}, \qquad (1)$$

where ω_{Pump} is the frequency of the incident photon and ω_{Signal} and ω_{Idler} are the frequencies of the two downconverted photons, and the conservation of momentum,

$$\vec{k}_{\text{Pump}} = \vec{k}_{\text{Signal}} + \vec{k}_{\text{Idler}}, \qquad (2)$$

where $\vec{k}_{Pump}$, $\vec{k}_{Signal}$ and $\vec{k}_{Idler}$ are the pump, signal and idler wave vectors, respectively.

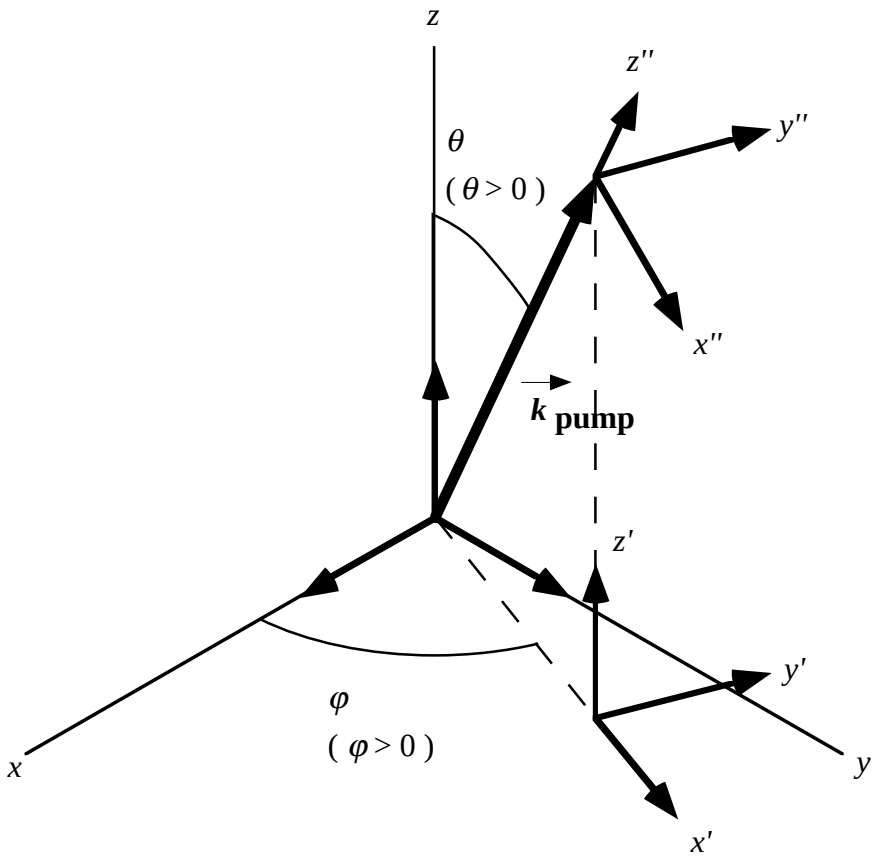

Figure 1. The crystal axes and the laboratory frame axes
x , y , z : crystal dielectric axes (optical plane is x-z plane, $n_Z > n_Y > n_X$)
x' , y' , z' : rotated axes (rotation angle φ, about the axis z)
x'' , y'' , z'' : laboratory frame axes (rotation angle φ, about the axis y')

Using spherical coordinates, the pump wave vector is expressed in the crystal principal dielectric axes $\hat{x}$, $\hat{y}$, $\hat{z}$ with the polar and azimuthal angles θ_{Pump} and φ_{Pump} defined as shown in Fig. 1. In uniaxial crystals there is only one axis allowing symmetry of revolution, so the direction of the pump can be specified by a single angle, θ_{Pump}. Thus, for uniaxial crystals the result of the calculations will not depend on the azimuthal angle, φ_{Pump}. However, for biaxial crystals, which lack that symmetry, two angles are required. The angles are defined here according to the Positive Nonlinear Optics Frame convention of Roberts [5].

Since the crystal dielectric axes are not convenient for calculating the resulting output, we express the signal and the idler wave vectors in the lab frame defined by the rotated axes $\hat{x}''$, $\hat{y}''$, $\hat{z}''$, as shown in Fig. 1. In the lab frame, the signal and idler wave vectors are:

$$\vec{k}_{\text{Pump}} = n_{\text{Pump}}(\theta_{\text{Pump}}, \varphi_{\text{Pump}}) \frac{\omega_{\text{Pump}}}{c} \hat{s}_{\text{Pump}}$$

$$\vec{k}_{\text{Signal}} = n_{\text{Signal}}(\theta_{\text{Signal}}, \varphi_{\text{Signal}}) \frac{\omega_{\text{Signal}}}{c} \hat{s}_{\text{Signal}} \qquad (3)$$

$$\vec{k}_{\text{Idler}} = n_{\text{Idler}}(\theta_{\text{Idler}}, \varphi_{\text{Idler}}) \frac{\omega_{\text{Idler}}}{c} \hat{s}_{\text{Idler}}$$

where n_i (i = Pump, Signal, Idler) are the refractive indices for the photons (for their individual states of polarization) in the given direction of propagation $\hat{s}_i$. Here θ_{Pump} is the angle between $\hat{s}_{\text{Pump}}$ and the $\hat{z}$ axis, while φ_{Pump} is the azimuthal angle (about $\hat{z}$) from the $\hat{x}$ axis to $\hat{s}_{\text{Pump}}$ in the x-y plane. For the downconversion beams, the opening angles θ_{Signal} and θ_{Idler} are specified relative to $\hat{s}_{\text{Pump}}$, and the azimuthal angles φ_{Signal} and φ_{Idler} refer to rotations in the plane normal to $\hat{s}_{\text{Pump}}$ (see Figure 2.)

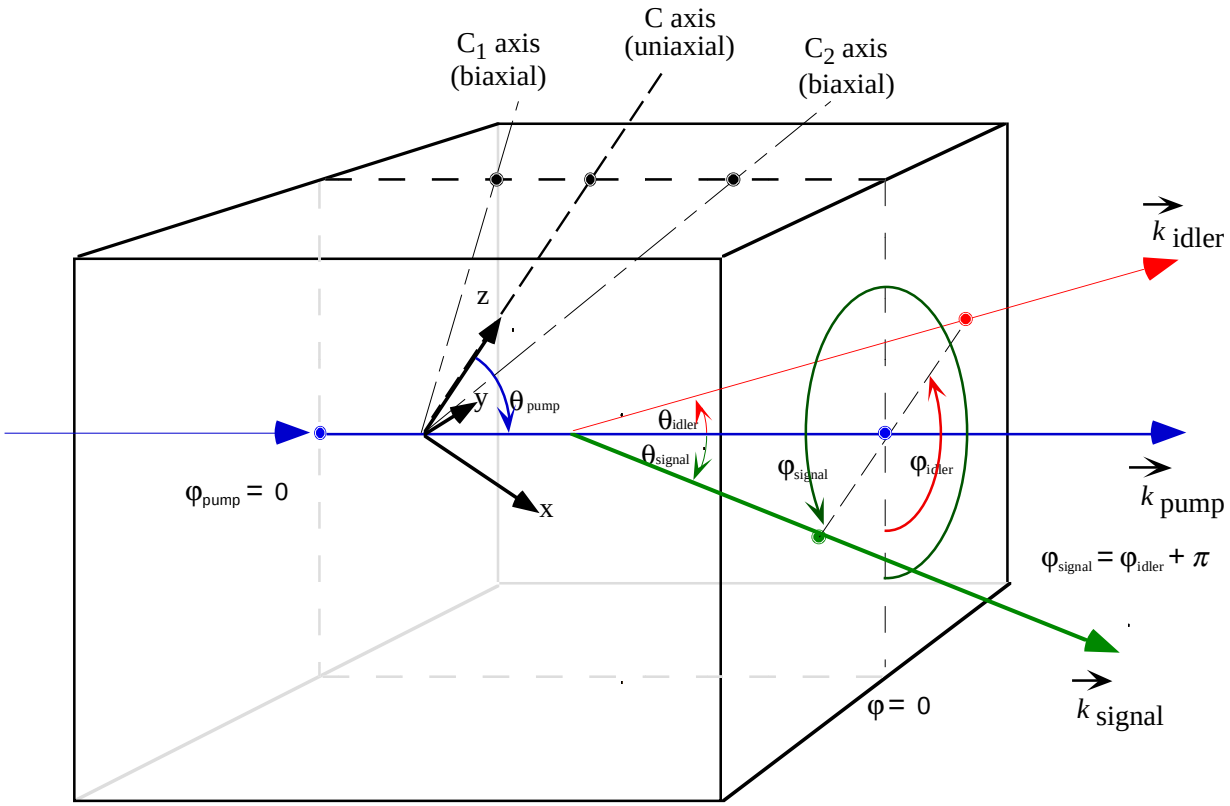

Figure 2. Another view of the crystal and laboratory frame coordinates, showing a typical experimental arrangement for parametric downconversion within a crystal. In this figure, the x-z plane ($\varphi_{Pump} = 0$ plane) is in the plane of the page; for uniaxial crystals, this choice can always be made, but for biaxial crystals, this drawing represents a special case in which the crystal axes C_1, C_2, and the pump beam all lie in the plane of the page. The signal beam is emerging low and towards the viewer, while the idler beam is propagating to high and away from the viewer. The azimuthal angles φ_{Signal} and φ_{Idler} are measured from the x-z plane. Dots indicate the points where the rays intersect the surface of the crystal.

The cosine vectors of the propagation direction $\hat{s}$ are: $s_x = \sin\theta\cos\varphi$, $s_y = \sin\theta\sin\varphi$ and $s_z = \cos\theta$. Note that the pump direction is specified with respect to the crystal axis (or axes) in the xyz frame via

$$\hat{s}_{\text{Pump}} = \begin{pmatrix} \sin\theta_{\text{Pump}}\cos\varphi_{\text{Pump}} \\ \sin\theta_{\text{Pump}}\sin\varphi_{\text{Pump}} \\ \cos\theta_{\text{Pump}} \end{pmatrix}_{x,y,z}, \tag{4}$$

while the signal and idler beams are specified relative to the pump beam via

$$\hat{s}_{\text{Signal}} = \begin{pmatrix} \sin\theta_{\text{Signal}}\cos\varphi_{\text{Signal}} \\ \sin\theta_{\text{Signal}}\sin\varphi_{\text{Signal}} \\ \cos\theta_{\text{Signal}} \end{pmatrix}_{x'',y'',z''}, \quad \hat{s}_{\text{Idler}} = \begin{pmatrix} \sin\theta_{\text{Idler}}\cos\varphi_{\text{Idler}} \\ \sin\theta_{\text{Idler}}\sin\varphi_{\text{Idler}} \\ \cos\theta_{\text{Idler}} \end{pmatrix}_{x'',y'',z''}. \tag{5}$$

The transformation between coordinate systems is given by

$$\begin{pmatrix} x \\ y \\ z \end{pmatrix} = \begin{pmatrix} \cos\theta\cos\varphi & -\sin\varphi & \sin\theta\cos\varphi \\ \cos\theta\sin\varphi & \cos\varphi & \sin\theta\sin\varphi \\ -\sin\theta & 0 & \cos\theta \end{pmatrix} \begin{pmatrix} x'' \\ y'' \\ z'' \end{pmatrix} \tag{6}$$

$$\begin{pmatrix} x'' \\ y'' \\ z'' \end{pmatrix} = \begin{pmatrix} \cos\theta\cos\varphi & \cos\theta\sin\varphi & -\sin\theta \\ -\sin\varphi & \cos\varphi & 0 \\ \sin\theta\cos\varphi & \sin\theta\sin\varphi & \cos\theta \end{pmatrix} \begin{pmatrix} x \\ y \\ z \end{pmatrix}, \tag{7}$$

where $\theta = \theta_{\text{Pump}}$ and $\varphi = \varphi_{\text{Pump}}$.

The problem to be solved has variables: θ_{Pump}, φ_{Pump}, θ_{Signal}, φ_{Signal}, θ_{Idler}, φ_{Idler}, ω_{Pump}, ω_{Signal}, and ω_{Idler}. These are related by Eqs. (1) and (2) which yield one and three equations, respectively. Thus, we have nine variables related by four equations. Five variables can therefore be chosen as parameters to reduce the number of unknowns to equal the number of equations. The pump direction and frequency (as given by $\theta_{\text{Pump}}, \varphi_{\text{Pump}}$, and ω_{Pump}) can clearly be chosen as parameters. In addition, one of the downconverted photon frequencies can be chosen, as well as its azimuthal angle. (In our analysis ω_{Signal} and φ_{Signal} are selected.)

In general (for uniaxial and biaxial crystals), there are two different indices of refraction for a single direction of propagation. For uniaxial crystals, those are the "ordinary" and the "extraordinary" indices of refraction. For biaxial crystals, they are referred to as the "fast" and the "slow," where the fast index is the smaller of the two indices. Having two possible indices for each wavelength allows the phase-matching of $\vec{k}_{\text{Pump}}$, $\vec{k}_{\text{Signal}}$ and $\vec{k}_{\text{Idler}}$ to be achieved in several ways, for example:

$$\vec{k}_{\text{Pump}}(\text{fast}) = \vec{k}_{\text{Signal}}(\text{slow}) + \vec{k}_{\text{Idler}}(\text{slow})$$

$$\vec{k}_{\text{Pump}}(\text{fast}) = \vec{k}_{\text{Signal}}(\text{fast}) + \vec{k}_{\text{Idler}}(\text{slow}) \qquad (8)$$

$$\vec{k}_{\text{Pump}}(\text{fast}) = \vec{k}_{\text{Signal}}(\text{slow}) + \vec{k}_{\text{Idler}}(\text{fast}).$$

These are the most common phase-matching configurations, and are usually classified by type [6]. The first line of Eq. (8) where the signal and idler beams have similar polarizations is referred to as type-I phase-matching. The second and third lines are examples of type-II phase-matching, in which the signal and idler polarizations are orthogonal; the names "signal" and "idler" are arbitrary, and may be assigned to either the fast or the slow wave. While it is theoretically possible for the pump to be the slow ray, this does not usually lead to phase-matching in most materials.

Phase-matching in uniaxial crystals is often described in terms of the ordinary and extraordinary indices. For example, in a "positive uniaxial" crystal -- one for which the extraordinary ray travels slower than the ordinary ray – phase-matching is achieved with the following combinations of the ordinary and the extraordinary light:

$$\vec{k}_{\text{Pump}}(\text{o}) = \vec{k}_{\text{Signal}}(\text{e}) + \vec{k}_{\text{Idler}}(\text{e})$$

$$\vec{k}_{\text{Pump}}(\text{o}) = \vec{k}_{\text{Signal}}(\text{o}) + \vec{k}_{\text{Idler}}(\text{e}) \qquad (9)$$

$$\vec{k}_{\text{Pump}}(\text{o}) = \vec{k}_{\text{Signal}}(\text{e}) + \vec{k}_{\text{Idler}}(\text{o}).$$

We find the index of refraction $n(\hat{s})$ in a given direction $\hat{s} = (s_x, s_y, s_z)$ using the indicatrix equation given by *Fresnel's equation of wave normals*, expressed in terms of the crystal principal dielectric axes [7]:

$$\frac{s_x^2}{\frac{1}{n^2(\hat{s})} - \frac{1}{n_x^2}} + \frac{s_y^2}{\frac{1}{n^2(\hat{s})} - \frac{1}{n_y^2}} + \frac{s_z^2}{\frac{1}{n^2(\hat{s})} - \frac{1}{n_z^2}} = 0. \qquad (10)$$

Here n_x, n_y and n_z are the crystal principal refractive indices at a given wavelength. For a biaxial crystal, $n_x < n_y < n_z$, while for a uniaxial crystal, $n_x = n_y = n_o$ (ordinary) and $n_z = n_e$ (extraordinary). Equation (10) can be rewritten as:

$$x^2 - \left[s_x^2 \left(\frac{1}{n_y^2} + \frac{1}{n_z^2} \right) + s_y^2 \left(\frac{1}{n_x^2} + \frac{1}{n_z^2} \right) + s_z^2 \left(\frac{1}{n_x^2} + \frac{1}{n_y^2} \right) \right] x + \left[\frac{s_x^2}{n_y^2 n_z^2} + \frac{s_y^2}{n_x^2 n_z^2} + \frac{s_z^2}{n_x^2 n_y^2} \right] = 0 \qquad (11)$$

where $x = \frac{1}{n^2(\hat{s})}$. Solving for *x*, we obtain one solution for each possible polarization (fast or slow):

$$n_{fast} = \sqrt{\frac{2}{B + \sqrt{B^2 - 4C}}},$$

$$n_{slow} = \sqrt{\frac{2}{\sqrt{B - \sqrt{B^2 - 4C}}}}, \tag{12}$$

with

$$B = \left[s_x{}^2 \left(\frac{1}{n_y^2} + \frac{1}{n_z^2} \right) + s_y{}^2 \left(\frac{1}{n_x^2} + \frac{1}{n_z^2} \right) + s_z{}^2 \left(\frac{1}{n_x^2} + \frac{1}{n_y^2} \right) \right]$$

$$C = \left[\frac{s_x{}^2}{n_y^2 \cdot n_z^2} + \frac{s_y{}^2}{n_x^2 \cdot n_z^2} + \frac{s_z{}^2}{n_x^2 \cdot n_y^2} \right].$$

To solve the phase-matching problem, we choose a crystal and type of phase-matching. The only data needed are the indices of refraction of the crystal. As already mentioned, we can select the pump frequency and direction, (ω_{Pump}, θ_{Pump}, φ_{Pump}) and the signal frequency and azimuthal angle (ω_{Signal}, φ_{Signal}). It is also clear from Eq. (2) that the three wave vectors must lie in a plane so:

$$\varphi_{\text{Idler}} = \varphi_{\text{Signal}} + \pi. \tag{13}$$

This relation makes one of the three component equations represented by Eq. (2) redundant. So now we have three equations and three unknowns remaining. Of these Eq. (1) simply relates ω_{Idler} to ω_{Pump} and ω_{Signal}, leaving just two coupled equations and two unknowns.

II. 2. Solving the equations

The remaining variables, θ_{Signal} and θ_{Idler} must be found simultaneously using Eq. (2). This problem is complex because the index of refraction depends on the wave vector direction, so in the general biaxial case, we must solve Eq. (10) to find an index. This affects the magnitude of the wave vector as shown in Eq. (3) requiring that we solve Eq. (2) using both Eqs. (3) and (10). Because this problem has no analytic solution, it requires an iterative search routine. We can deal with this situation three different ways. First, we may use two equations of Eq. (2) to

find a relation between θ_{Signal} and θ_{Idler} and then use the remaining equation of Eq. (2) to find its root with a root finding subroutine (one equation and one unknown). Second, we may rewrite Eq. (2) as

$$\left|\Delta\vec{k}\right| = 0, \tag{14}$$

where

$$\Delta\vec{k} = \vec{k}_{\text{Pump}} - \vec{k}_{\text{Signal}} - \vec{k}_{\text{Idler}}, \tag{15}$$

and find its minimum as a function of θ_{Signal} and θ_{Idler}. A final method is to apply a one-dimensional minimization algorithm after obtaining a relation between θ_{Signal} and θ_{Idler}.

The first method finds the $\Delta\vec{k}$ minimum by resolving Eq. (14) into the three following equations:

$$\Delta k_x = 0 \tag{16}$$

$$\Delta k_y = 0 \tag{17}$$

$$\Delta k_z = 0 \tag{18}$$

Then a root-finding subroutine is needed to solve these equations. This method works well for uniaxial crystals, but produces erroneous results for some biaxial crystals: $\Delta k_x = 0$, $\Delta k_y = 0$ and $\Delta k_z = 0$ can be solved independently, but the resulting $\left|\Delta\vec{k}\right|$ may not necessarily equal zero. This can happen because the θ_{Signal} and θ_{Idler} values required for $\Delta k_x = 0$ can be different from those required for $\Delta k_y = 0$ and $\Delta k_z = 0$. Therefore, although this method is faster than the other methods, it requires an independent check of $\left|\Delta\vec{k}\right| = 0$. Furthermore, in the case of a finite length crystal it is difficult to determine whether phase-matching is allowed, because one can have phase-matching even when $\left|\Delta\vec{k}\right| \neq 0$.

The second method, treats $\Delta\vec{k}$ as a vector quantity and finds the minimum of $\left|\Delta\vec{k}\right| = f\left(\theta_{\text{Signal,}}\theta_{\text{Idler}}\right)$. For the idealized case of an infinitely long crystal and infinitely wide pump beam, $\left|\Delta\vec{k}\right| = 0$ is required for phase-matching, because the interaction Hamiltonian contains an integral over all space [8] producing a delta function:

$$\iiint_V e^{i\cdot\Delta\vec{k}\cdot\vec{r}}\, d^3r \propto \delta(\Delta\vec{k}). \tag{19}$$

However, for a finite crystal length *L* and a Gaussian transverse pump intensity profile of finite width *W*, it is possible for downconversion to occur even when $\Delta\vec{k} \neq \vec{0}$, that is, with imperfect phase-matching. In this case, the interaction Hamiltonian integral yields the phase-matching function:

$$\Phi = \exp\left(-\frac{1}{2}W^2\left(\Delta k_x^2 + \Delta k_y^2\right)\right)\cdot\left(\frac{\sin\left(\frac{1}{2}L\Delta k_z\right)}{\frac{1}{2}L\Delta k_z}\right)^2 . \qquad (20)$$

This function is a weighting function for the intensity of the emitted downconversion that has a maximum value of 1 for $\left|\Delta\vec{k}\right| = 0$, and falls to zero as the phase mismatch $\left|\Delta\vec{k}\right|$ increases. We may then arbitrarily say that phase-matching occurs for values of $\left|\Delta\vec{k}\right|$ that yield $\Phi \geq \frac{1}{2}$ (see Figure 3). This corresponds to $\left|\Delta k_z\right| \leq \frac{2.783}{L}$ in the direction of pump propagation $\left(\Delta k_{\text{transverse}} = 0\right)$ or $\left|\Delta k_{\text{transverse}}\right| \leq \frac{1.177}{W}$ in the plane orthogonal to pump direction $\left(\Delta k_z = 0\right)$. For this situation, the goal of our method is still to find the minimum of $\left|\Delta\vec{k}\right|$ as a function of two variables, θ_{Signal} and θ_{Idler}, but we now must also evaluate the resulting value of Φ and determine whether $\Phi \geq \frac{1}{2}$ or not.

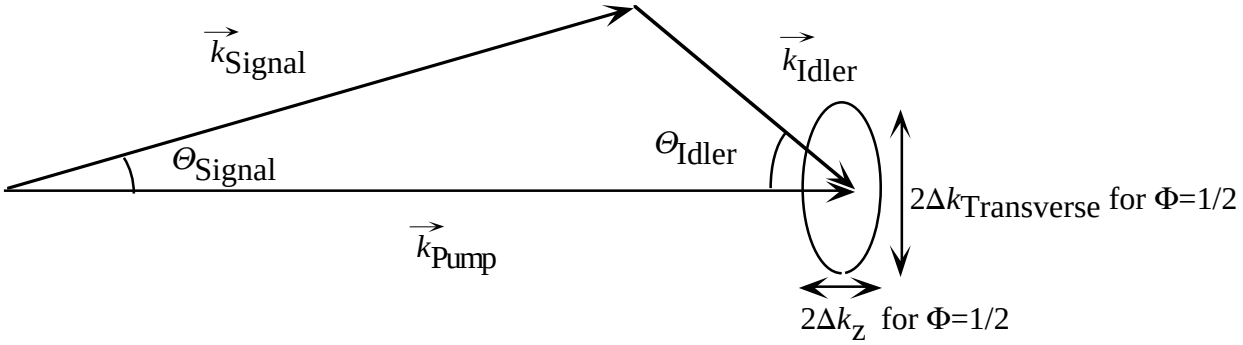

Figure 3. Imperfect phase-matching of the pump, signal, and idler propagation vectors.

Because there is no general analytical method to find the minimum value of $\left|\Delta\vec{k}\right|$ for each possible signal angle under a given set of pumping conditions, we search for this minimum iteratively, via a computer algorithm. This method is slower than the first, but produces more reliable results for both uniaxial and biaxial crystals. This method is implemented in our computer program (see Section III) as follows :

1. Set the value of $\lambda_{\text{Pump}}, \theta_{\text{Pump}}, \varphi_{\text{Pump}}$, λ_{Signal} and φ_{Signal}.
2. Calculate $\vec{k}_{\text{Pump}}$.
3. Calculate λ_{Idler} and φ_{Idler} (cf. Eq. (1) and Eq. (13)).
4. Initialize both the unknown θ_{Signal} and θ_{Idler} to the value *S* times 0.03 radian, where *S* is a scale factor chosen by the user. Alternatively, after the first iteration the user may

choose to initialize these variables with the optimum values found in the previous iteration.

5. Call UNCMND, a two-dimensional minimization routine which returns the minimum value of $\left|\Delta\vec{k}\right|$ and the optimum phase-matching values of θ_{Signal} and θ_{Idler} which correspond to this minimum. UNCMND computes $\left|\Delta\vec{k}\right|$ and its first derivative, and uses Newton's method to find the zero of the first derivative[1].
6. Write these values to an output file.
7. Increment λ_{Signal} or φ_{Signal} and go to step 3.

The third method for solving Eq. (2) begins by rewriting it as follows:

$$n_{\text{Idler}}\frac{\omega_{\text{Idler}}}{\omega_{\text{Signal}}}\sin\left(\theta_{\text{Idler}}\right)=n_{\text{Signal}}\sin\left(\theta_{\text{Signal}}\right), \tag{21}$$

$$n_{\text{Idler}}\frac{\omega_{\text{Idler}}}{\omega_{\text{Signal}}}\cos\left(\theta_{\text{Idler}}\right)=n_{\text{Pump}}\frac{\omega_{\text{Pump}}}{\omega_{\text{Signal}}}-n_{\text{Signal}}\cos\left(\theta_{\text{Signal}}\right). \tag{22}$$

By adding the squares of these two equations, one obtains:

$$n_{\text{Idler}}\frac{\omega_{\text{Idler}}}{\omega_{\text{Signal}}}=\sqrt{n_{\text{Signal}}^2+n_{\text{Pump}}^2\frac{\omega_{\text{Pump}}^2}{\omega_{\text{Signal}}^2}-2n_{\text{Pump}}n_{\text{Signal}}\frac{\omega_{\text{Pump}}}{\omega_{\text{Signal}}}\cos\left(\theta_{\text{Signal}}\right)}. \tag{23}$$

Then, using Eq.(23), Eq. (21) can be rewritten as:

$$\theta_{\text{Idler}}=\arcsin\left(\frac{n_{\text{Signal}}\sin(\theta_{\text{Signal}})}{\sqrt{n_{\text{Signal}}^2+n_{\text{Pump}}^2\frac{\omega_{\text{Pump}}^2}{\omega_{\text{Signal}}^2}-2n_{\text{Signal}}n_{\text{Pump}}\frac{\omega_{\text{Pump}}}{\omega_{\text{Signal}}}\cos(\theta_{\text{Signal}})}}\right) \tag{24}$$

to provide a relation between the two unknowns. We can then use a one dimensional minimization function for $\Delta\vec{k}$. Although it can save calculation time, this method was not implemented because it assumes θ_{Signal} is given by a definite relation to θ_{Idler}(i.e. perfect phase-matching) and so it does not lend itself to finding output spreading where $\Delta\vec{k}\neq 0$.

[1] UNCMND is a public-domain FORTRAN routine available at the following web site maintained by NIST:
http://math.nist.gov/cgi-bin/gams-serve/list-module-components/NMS/UNCMND/5673

III. Practice: computational results

We have implemented the methods above in a FORTRAN program designed to solve the phase-matching problem for a wide variety of pumping conditions and crystal materials. The program may be freely downloaded from the web and is capable of generating data for the following kinds of plots (*f* indicates function of):

1. 2D Plot, $n_x, n_y, n_z = f(\lambda_{\text{Pump}})$
2 .3D Plot, $n_{\text{slow}} - n_{\text{fast}} = f(\theta_{\text{Signal}}, \varphi_{\text{Signal}})$
3. 3D Plot, $\Delta k_{\text{minimum}} = f(\theta_{\text{Signal}}, \varphi_{\text{Signal}})$
4. 3D Plot, phase-matching function $\Phi = f(\Delta k_{\text{tranverse}}, \Delta k_z)$
5. 2D Plot, θ_{Signal} *vs.* θ_{Idler} (λ_{Signal} fixed) for a chosen value of the phase-matching function
6. Polar plot, (optimum θ_{Signal} ,optimum θ_{Idler}) $= f(\varphi_{\text{Signal}})$
7. 2D Plot, optimum $\theta_{\text{Signal}} = f(\lambda_{\text{Signal}})$ at chosen φ_{Signal} with spreading in θ_{Signal} and φ_{Signal} , θ_{Idler} and φ_{Idler} fixed
8. 2D Plot, optimum $\theta_{\text{Signal}} = f(\lambda_{\text{Signal}})$ at chosen φ_{Signal} with spreading in θ_{Signal} and φ_{Signal}
9. 3D plot, phase-matching function $\Phi = f(\lambda_{\text{Signal},} \theta_{\text{Signal},})$
10. 3D plot, phase-matching function $\Phi = f(\lambda_{\text{Signal},} \varphi_{\text{Signal},})$

We now proceed to give examples and discussion of the results for each of these options.

III. 1. 2D Plot, $n_x, n_y, n_z = f(\lambda_{\text{Pump}})$

This plots the most basic information available for a specific crystal material, namely, the variation of the indices of refraction with wavelength. The program includes the coefficients in the Sellmeier-type index dispersion relations [9] for a number of common nonlinear optical materials, drawn from references that are cited in comment lines in the code. Plots of this kind provide the first clue as to whether any phase-matching will be possible for a particular combination of pump, signal, and idler wavelengths. Such a plot for BBO is shown in Figure 4.

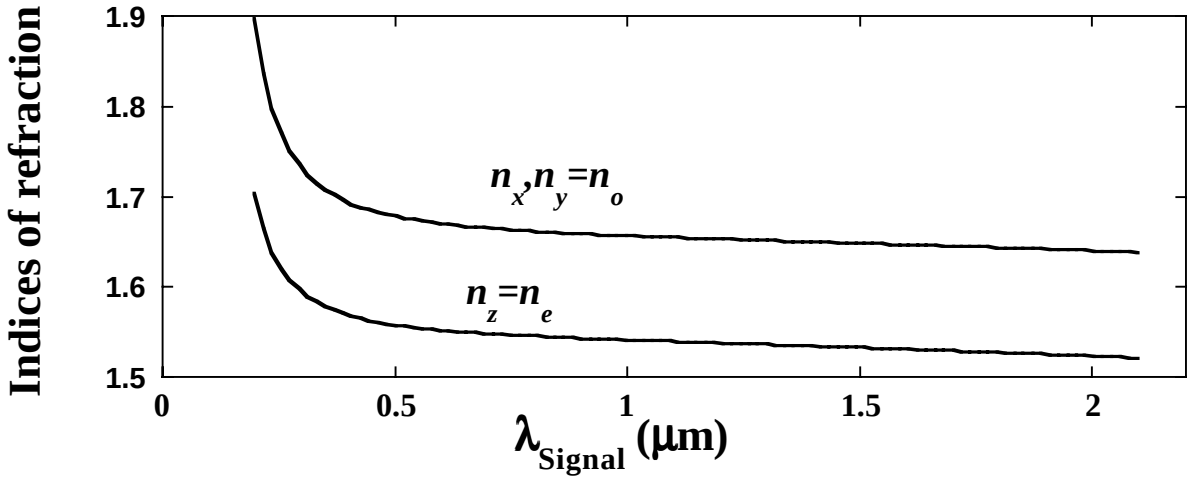

Figure 4. Indices of refraction versus wavelength for BBO, a negative uniaxial crystal. The graph indicates that "extraordinary" waves (polarized parallel to the optical axis *z*) travel faster than "ordinary" waves (polarized transverse to this axis).

III. 2. 3D Plot, $n_{\text{slow}} - n_{\text{fast}} = f(\theta_{\text{Signal}}, \varphi_{\text{Signal}})$

Although it is fairly simple to determine crystal configurations that produce phase-matching in a uniaxial crystal (because there is only a single variable, θ_{Pump}), determining phase-matching regions in a biaxial crystal, such as $KNbO_3$ is more complex [10-12]. To determine the effect of both variables (θ_{Pump} and φ_{Pump}), graphs of $n_{\text{Slow}} - n_{\text{Fast}}$ versus θ_{Pump} and φ_{Pump} can be produced (Fig. 5). As will be seen in the next option, phase-matching usually occurs where $n_{\text{Slow}} - n_{\text{Fast}}$ differs significantly from zero.

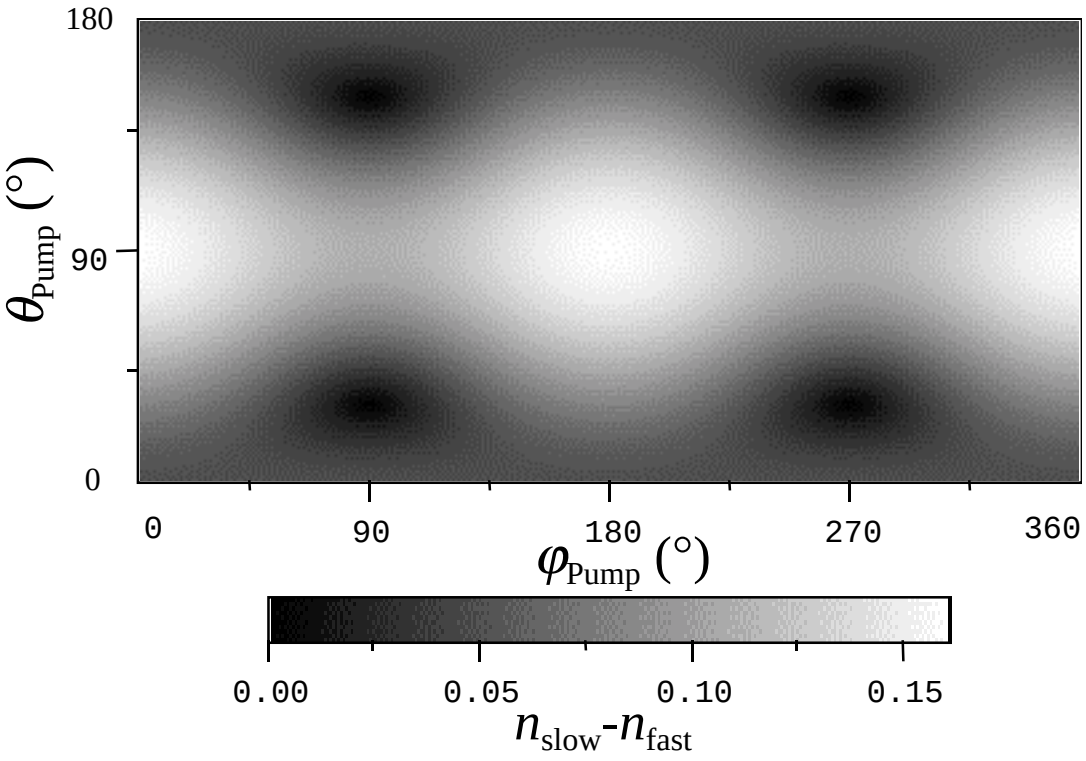

Figure 5. $n_{\text{Slow}} - n_{\text{Fast}}$ versus θ_{Pump} and φ_{Pump} in a $KNbO_3$ crystal with $\lambda_{\text{Pump}} = 0.633\mu\text{m}$.

III. 3. 3D Plot, $\Delta k_{\text{minimum}} = f(\theta_{\text{Signal}}, \varphi_{\text{Signal}})$

Graphs of the minimum value of $\left|\Delta\vec{k}\right|$ versus θ_{Pump} and φ_{Pump} can also be produced (see Figure 6.) One may notice the similarity between Figures 5 and 6. If $n_{\text{Slow}} - n_{\text{Fast}} \cong 0$, then $\Delta k_{\text{minimum}}$ is large, while if $n_{\text{Slow}} - n_{\text{Fast}}$ is large, then $\left|\Delta\vec{k}_{\text{minimum}}\right| \cong 0$. It is clear that some difference between n_{Slow} and n_{Fast} is required for phase-matching. These plots can be then used to quickly determine which crystal configurations lead to phase-matching.

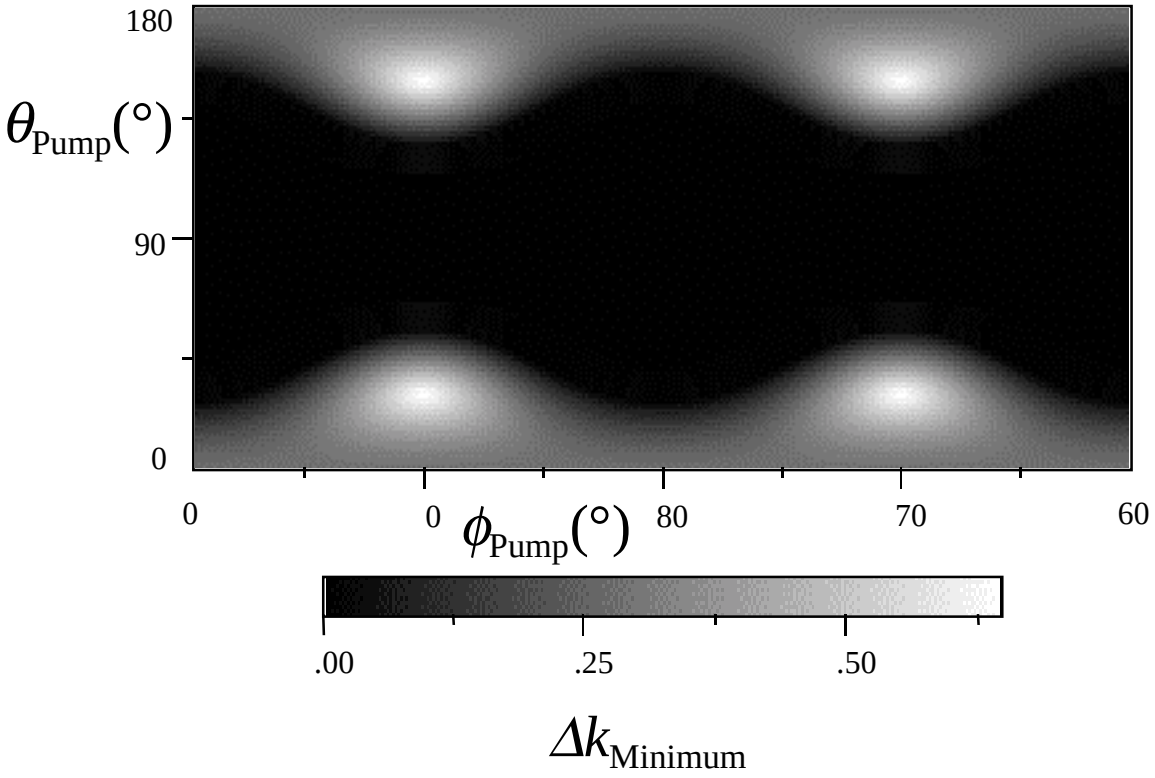

Figure 6. $\left|\Delta\vec{k}\right|$ versus θ_{Pump} and φ_{Pump} in a $KNbO_3$ crystal with $\lambda_{\text{Pump}} = 0.633\mu\text{m}$ and $\lambda_{\text{Signal}} = 0.950\,\mu\text{m}$.

III. 4. 3D Plot, Phase-matching function $\Phi = f(\Delta k_{\text{tranverse}}, \Delta k_z)$

For crystals of finite length, the signal and idler vectors need not sum exactly to the pump vector for some downconversion to occur (see Figure 3). For these cases, the downconversion intensity will be weighted by the phase-matching function Φ, as defined in Eq. (20). This option generates data for plots of Φ (see Figure 7), indicating the regions of momentum-space around the pump vector into which the sum of the signal and idler vectors must fall for downconversion to occur. The downconversion intensity will be highest for the central regions where $\Phi \cong 1$ (i.e. $\left|\Delta\vec{k}\right| \cong 0$) and lowest for the outer regions where $\Phi \cong 0$. Note that the longer the crystal, the more constricted the phase-matching region becomes in the $\hat{z}$ direction. Similarly, a wider pump beam would restrict the phase-matching region, but in the transverse direction.

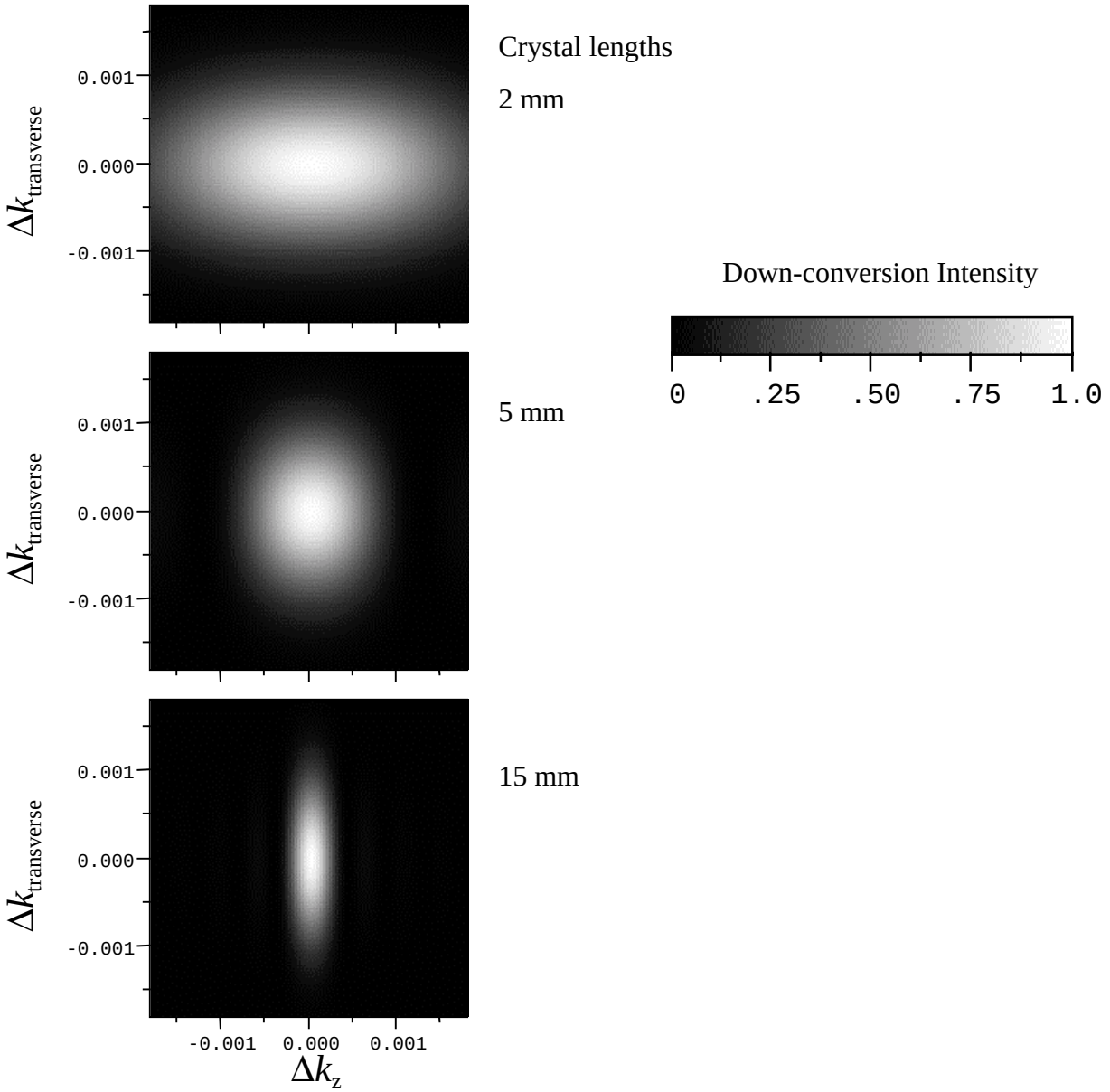

Figure 7 Phase-matching function for KDP crystals of three different lengths and constant pump beam width of 2 mm (FWHM).

III. 5. 2D Plot, θ_{Signal} *vs.* θ_{Idler} (λ_{Signal} fixed) for a chosen value of the phase-matching function

For a crystal of finite length and pump beam of finite width, there are many combinations of signal and idler opening angles that can lead to downconversion at a given pair of signal and idler wavelengths. This option generates a plot of all possible combinations of θ_{Signal} *vs.* θ_{Idler} which result in the phase-matching function falling to some specific value, say, $\Phi = 0.5$, for a particular pair of fixed downconversion wavelengths (see Figure 8).

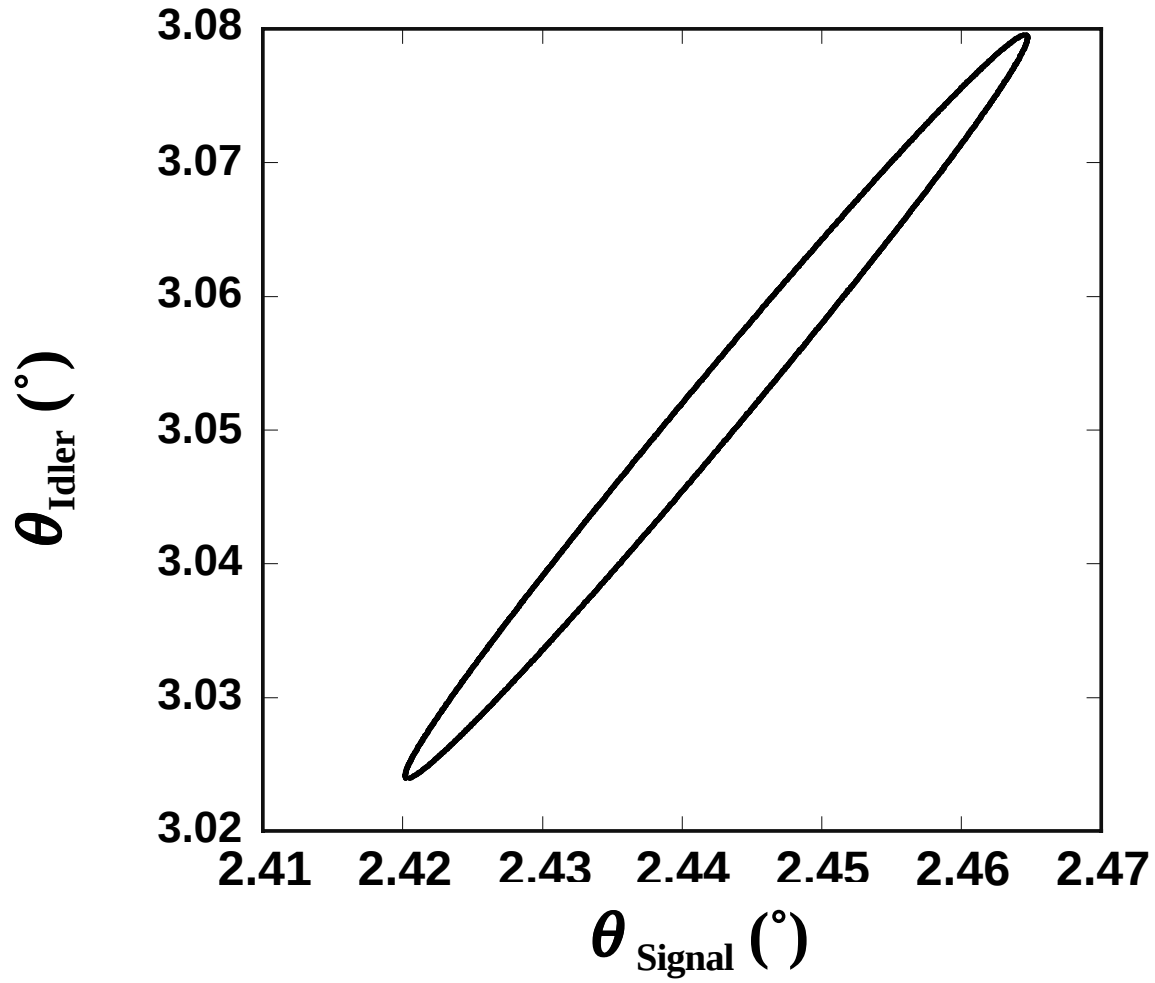

Figure 8. θ_{Signal} versus θ_{Idler} (Φ =0 .5) for a KDP crystal (5mm crystal length and 2 mm pump width) with $\lambda_{\text{Pump}} = 0.351\mu\text{m}$, $\varphi_{\text{Pump}} = 0^{\circ}$, $\theta_{\text{Pump}} = 52^{\circ}$, $\lambda_{\text{Signal}} = 0.633\mu\text{m}$, $\varphi_{\text{Signal}} = 0^{\circ}$.

III. 6. Polar plot, (Optimum θ_{Signal}, Optimum θ_{Idler}) = $f(\varphi_{Signal})$

To map the down-conversion output, this option produces two-dimensional graphs of the signal and idler output directions for a given signal frequency (Figure 9). This graph corresponds to a single crystal configuration (θ_{Pump} and ω_{Pump} are fixed with φ_{Pump} arbitrary because BBO is uniaxial) and a single ω_{Signal} (which can be used with Eq. (1) to calculate ω_{Idler}). The configuration in Figure 9 was chosen because it shows both the collinear (θ_{Idler} =θ_{Signal}=0) and non-collinear cases. Both the internal and external angles for the emission are calculated, although only the internal results are shown below. Multiple plots of this kind with different signal and idler frequencies can be examined if more complete results of the downconversion are desired.

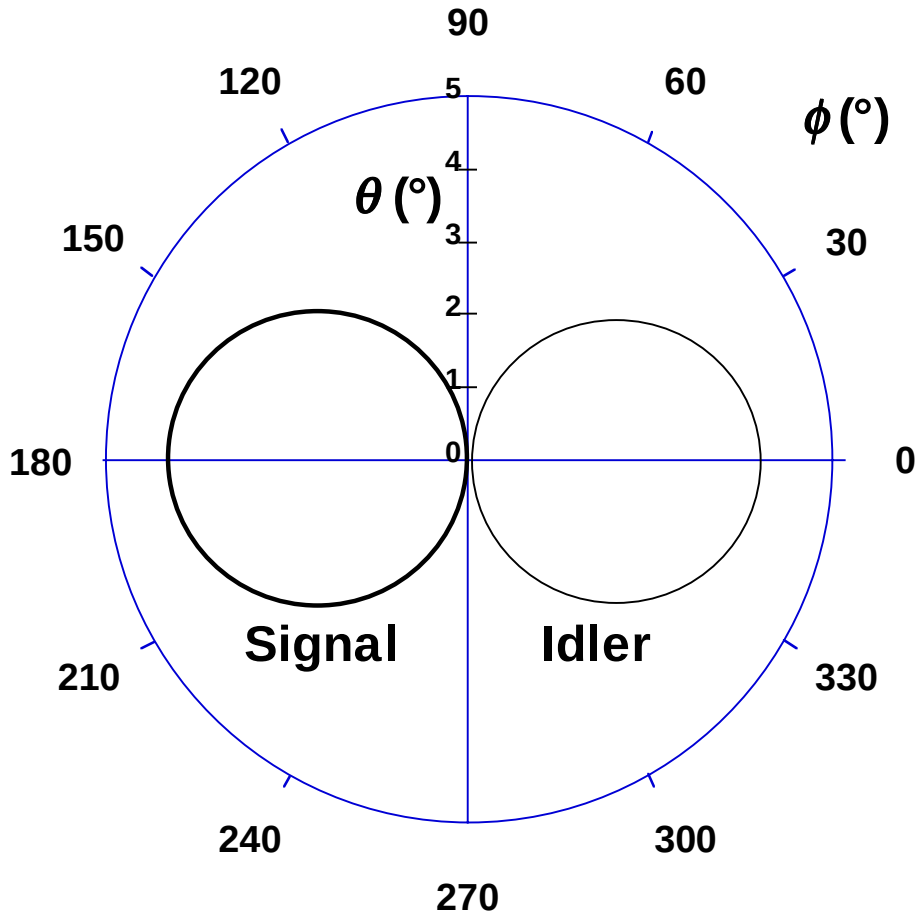

Figure 9. Polar plot of the direction of signal and idler output photons ($\lambda_{Signal,Idler} = 0.702\,\mu m$) for θ_{Pump}=49.2°, λ_{Pump}=0.351 μm from a BBO crystal. The pump beam propagates out of the page at the origin.

III. 7. 2D Plot, Optimum $\theta_{\text{Signal}} = f(\lambda_{\text{Signal}})$ at chosen φ_{Signal} with spreading in θ_{Signal} and φ_{Signal}, θ_{Idler} and φ_{Idler} fixed

For any given pair of conjugate signal and idler wavelengths, there may exist an optimum pair of emission angles $\theta_{\text{Signal}}, \theta_{\text{Idler}}$ producing perfect phase-matching (i.e. satisfying Eq. (2) and yielding Φ=1). Downconversion will be strongest for these optimum combinations of wavelengths and angles. This option provides data for plotting the optimum signal angle as a function of signal wavelength, as shown in Figure 10. For type-I downconversion, the names "signal" and "idler" are completely arbitrary, so that this is in fact a graph of both the signal and idler emission angles. For type-II downconversion, one may find the idler angles by running the option again and choosing the "signal" (now really the idler) to be the slow wave instead of the fast wave, or vice versa. Both the internal and external angles are reported (Figure 10 displays on internal angles). The opening angles can be plotted for any choice of emission plane, such as $\varphi_{\text{Signal}} = 0^{\circ}$.

If the crystal were infinitely long, downconversion would occur only at these optimal combinations of wavelength and angle. For crystals of finite length, however, some emission will occur in a range of angles about the optimum for each wavelength. The broader the phase-matching function, the larger this range of angles becomes, as one might guess from examining Figures 3 and 7. Therefore, option 7 also provides a first-order estimate of this spreading in both θ_{Signal} and φ_{Signal} as a function of wavelength. For each signal wavelength, the spreading in the signal angles is calculated assuming that the conjugate idler photon is emitted at precisely the optimum opening angle for its wavelength, so that only θ_{Signal} and φ_{Signal} are allowed to vary. The largest non-optimal values of θ_{Signal} and φ_{Signal} that result in Φ falling to some specific value, say, $\Phi = 0.5$, are found, and the difference between these non-optimal angles and the optimal angles are reported in the data set as "spreads." They may be used to construct error-bars or plotted independently as in Figure 10.

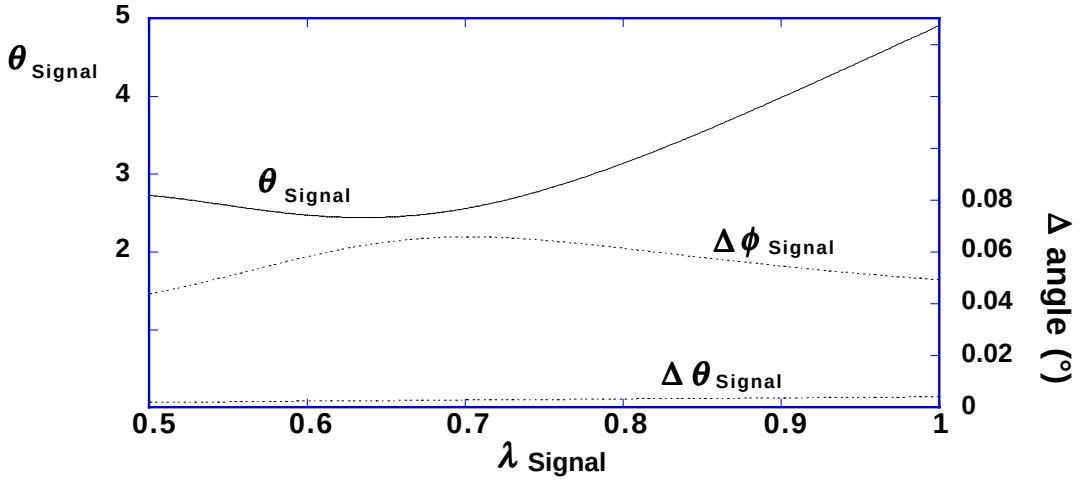

Figure 10. Upper curve shows optimum $\theta_{\text{Signal}} = f(\lambda_{\text{Signal}})$, while the lower two curves show the spreads in θ_{Signal} and φ_{Signal}, with θ_{Idler} and φ_{Idler} fixed, Φ=0.5. All curves for a 5mm long KDP crystal and 2 mm pump beam width, λ_{Pump}=0.351 μm, θ_{Pump}=52°, ϕ_{Pump}=0°, and ϕ_{Signal}=0°.

III. 8. 2D Plot, Optimum $\theta_{\text{Signal}} = f(\lambda_{\text{Signal}})$ at chosen φ_{Signal} with spreading in θ_{Signal} and φ_{Signal} .

This option is the same as option 7, but the spreads in θ_{Signal} at each wavelength are computed in an iterative fashion that allows both the signal and the idler to be emitted at a non-optimal opening angle (Figure 11). This provides a more realistic estimate for the spreads than that given by the previous option, but also requires more computing time. However, the spread in φ_{Signal} is computed exactly as in the previous option. For if the idler were not constrained to be emitted in the plane chosen by the user (say, $\varphi_{\text{Idler}} = 180^{\circ}$ corresponding to the choice of optimum $\varphi_{\text{Signal}} = 0^{\circ}$) then the sequence of iterations would simply map out the entire circle of emission for both the signal and the idler. As in option 7, the spreads that result in Φ falling to some user-defined "target" value like $\Phi = 0.5$ are computed.

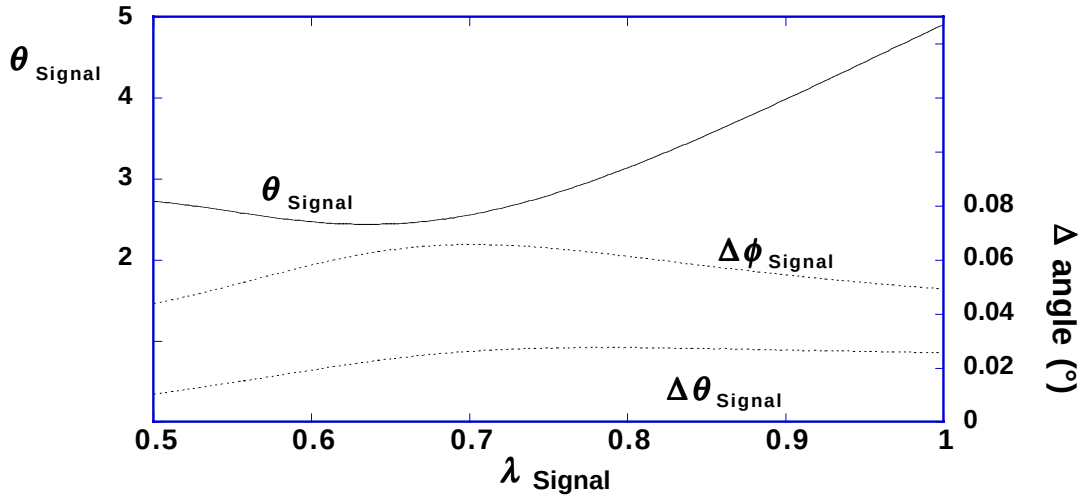

Figure 11. Upper curve shows optimum $\theta_{\text{Signal}} = f(\lambda_{\text{Signal}})$, while the lower two curves show the spreads in θ_{Signal} and φ_{Signal} , with φ_{Idler} fixed, Φ=0.5, for a 5mm crystal length and 2 mm pump width. Here θ_{Idler} is allowed to vary, as opposed to Figure 10 where θ_{Idler} was fixed. This difference produces a larger spread in θ_{Signal} All curves for a 5mm long KDP crystal and 2 mm pump beam width, λ_{Pump}=0.351 μm, θ_{Pump}=52°, ϕ_{Pump}=0°, and ϕ_{Signal}=0°.

III. 9. 3D plot, Phase-matching function $\Phi = f(\lambda_{\text{Signal,}}\theta_{\text{Signal,}})$

In this option, the value of the phase-matching function is computed for the entire range of signal wavelength and angle combinations, within the domain of validity of the Sellmeier coefficients for the chosen crystal. This is done by repetition of option 8, with the "target" value of Φ incremented from 0.1 to 1. Because the phase-matching function is a weight function for the emission of downconverted pairs, a 3-D plot of $\Phi(\lambda_{\text{Signal,}}\theta_{\text{Signal}})$ can serve as a crude picture of the relative intensity of the downconversion as a function of wavelength and angle (see Figures 12). The intensity will be highest for the optimum phase-matching combinations that result in $\Phi = 1$. It is important to note that such plots cannot provide completely accurate pictures of the downconversion intensity, since the probability of downconversion is also affected by the strength of the nonlinear electric susceptibility -- another frequency dependent quantity. However, if the values of Φ are compared over a range of frequencies with nearly constant susceptibility, then their interpretation as relative intensities for the downconversion should be valid over that range.

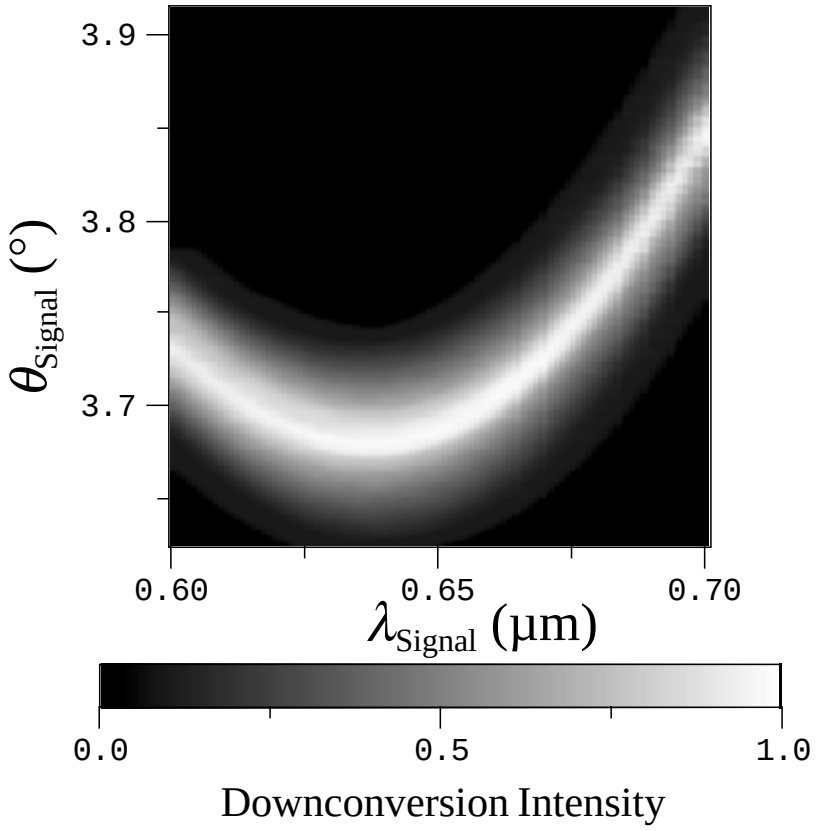

Figure 12. $\Phi = f(\lambda_{\text{Signal,}}\theta_{\text{Signal}})$ for a KDP crystal (5mm crystal length and 2 mm pump width) with $\lambda_{\text{Pump}} = 0.351\mu\text{m}, \varphi_{\text{Pump}} = 0^{\circ}, \theta_{\text{Pump}} = 52^{\circ}, \varphi_{\text{Signal}} = 0^{\circ}$. (Here θ_{Signal} is an external angle.)

III. 10. 3D plot, Phase-matching $\Phi = f(\lambda_{\text{Signal,}}\varphi_{\text{Signal,}})$

This option shows the variation of Φ as a function of signal wavelength and signal azimuthal angle (rather than opening angle as in the previous option), assuming that the azimuthal angle of the idler is fixed (as in options 7 and 8.) A 3D plot of the results (shown in Figure 13) can be interpreted as plots of relative downconversion intensity versus wavelength and azimuthal angle, with the same caveats as listed for option 9.

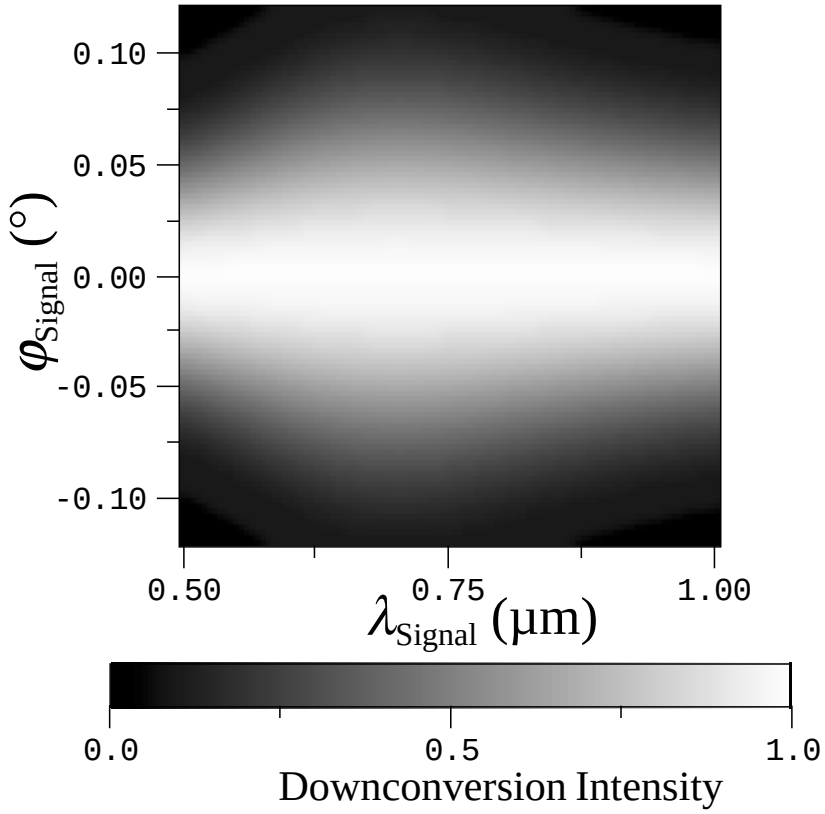

Figure 13. $\Phi = f(\lambda_{\text{Signal,}}\varphi_{\text{Signal}})$ for a KDP crystal (5mm crystal length and 2 mm pump width) with $\lambda_{\text{Pump}} = 0.351\mu\text{m}, \varphi_{\text{Pump}} = 0^{\circ}, \theta_{\text{Pump}} = 52^{\circ}$, and $\varphi_{\text{Signal}} = 0^{\circ}$

IV. Conclusion

The methods presented here for calculating both collinear and non-collinear phase-matching allows experimental configurations including either uniaxial or biaxial crystals to be modeled in detail. These computational techniques can provide preliminary answers to a variety of questions that must be asked about a particular downconversion source before it is constructed in the laboratory, such as "Over what range of wavelengths is downconversion possible? What should the 'cut' of the crystal's optical axis be? At what angles can we expect to find certain wavelengths emitted from the crystal?" and so on. To our knowledge, the program made available here is the first comprehensive scheme that can provide answers to such questions for both collinear and non-collinear phase-matching, and in both uniaxial and biaxial crystals. We hope that this method and its implementation will aid researchers in designing downconversion schemes that rely on these more complicated phase-matching conditions.

The computer program that performs these calculations is continually being improved. In the future we hope to make updated versions available which include the effects of curved pump wavefronts on the spatial profiles of the downconversion beams, as well as the effects of the extended-source nature of the downconversion region within the crystal.

References:

[1] L. Mandel, "Quantum Effects in One-Photon and Two-Photon Interference," in *More things in heaven and earth: A celebration of physics at the millennium*, edited by B. Bederson (Springer-Verlag, New York, 1999), p. 460.

[2] A. Zeilinger, "Experiment and the Foundations of Quantum Physics," in *More things in heaven and earth: A celebration of physics at the millennium*, edited by B. Bederson (Springer-Verlag, New York, 1999), p. 482.

[3] A. Migdall, "Correlated Photon Metrology Without Absolute Standards," *Physics Today* **52**, 41 (1999).

[4] A. Migdall, R. Datla, A. V. Sergienko, J. S. Orszak, and Y. H. Shih, "Measuring absolute infrared spectral radiance using correlated visible photons: Technique verification and measurement uncertainty," *Applied Optics* **37**, 3455 (1998).

[5] D. A. Roberts, "Simplified characterization of uniaxial and biaxial nonlinear optical crystals: A plea for standardization of nomenclature and convention," *IEEE Journal of Quantum Electronics* **28**, 2057 (1992).

[6] G. J. Zhang, S. Horinouchi, T. Kinoshita, and K. Sasaki, "Theoretical analysis of the spatial phase-matching loci for second-harmonic generation and multiwave-mixing interactions," *Applied Optics* **34**, 5301 (1995).

[7] A. Yariv and P. Yev, *Optical Waves in Crystals* (John Wiley & Sons, New York, 1984).

[8] Z. Y. Ou, L. J. Wang, and L. Mandel, "Vacuum effects on interference in two-photon down conversion," *Physical Review A* **40**, 1428 (1989).

[9] E. Hecht, *Optics* (Addison-Wesley, Reading, MA, 1989).

[10] B. Wyncke and F. Brehat, "Calculation of the effective second-order nonlinear coefficients along the phase-matching directions in acentric orthorhombic biaxial crystals," *Journal of Physics B* **22**, 363 (1989).

[11] B. Zysset, I. Biaggio, and P. Gunter, "Refractive indices of orthorhombic KNbO3," *Journal of the Optical Society of America B* **9**, 380 (1992).

[12] D. Y. Stepanov, V. D. Shigorin, and G. P. Shipulo, "Phase-matching directions in optical mixing in biaxial crystals having quadratic susceptibility," *Soviet Journal of Quantum Electronics* **14**, 1315 (1984).